

Fine-structures of planar deformation features in shocked olivine: A comparison between Martian meteorites and experimentally shocked basalts as an indicator for shock pressure

HPSTAR
858-2019

Atsushi TAKENOUCI ^{1,2*}, Takashi MIKOUCHI³, Takamichi KOBAYASHI⁴,
Toshimori SEKINE^{5,6}, Akira YAMAGUCHI ^{1,7}, and Haruka ONO ⁸

¹National Institute of Polar Research (NIPR), 10-3 Midori-cho, Tachikawa, Tokyo 190-8518, Japan

²Department of Basic Science, The University of Tokyo, 3-8-1 Komaba, Meguro-ku, Tokyo 153-8902, Japan

³The University Museum, The University of Tokyo, 7-3-1 Hongo, Bunkyo-ku, Tokyo 113-0033, Japan

⁴National Institute for Materials Science (NIMS), 1-1 Namiki, Tsukuba, Ibaraki 305-0044, Japan

⁵Center for High Pressure Science and Technology Advanced Research (HPSTAR), 1690 Cailun Rd, Pudong, Shanghai 201203, P.R. China

⁶Graduate School of Engineering, Osaka University, 2-1 Yamadaoka, Suita, Osaka 565-0871, Japan

⁷Department of Polar Science, School of Multidisciplinary Science, SOKENDAI (The Graduate University for Advanced Studies), Tachikawa, Tokyo 190-8518, Japan

⁸Department of Earth and Planetary Science, The University of Tokyo, 7-3-1 Hongo, Bunkyo-ku, Tokyo 113-0033, Japan

*Corresponding author. E-mail: takenouchia24@gmail.com

(Received 19 June 2018; revision accepted 27 June 2019)

Abstract—We performed shock recovery experiments on an olivine-phyric basalt at shock pressures of 22.2–48.5 GPa to compare with shock features in Martian meteorites (RBT 04261 and NWA 1950). Highly shocked olivine in the recovered basalt at 39.5 and 48.5 GPa shows shock-induced planar deformation features (PDFs) composed of abundant streaks of defects. Similar PDFs were observed in olivine in RBT 04261 and NWA 1950 while those in NWA 1950 were composed of amorphous lamellae. Based on the present results and previous studies, the width and the abundance of lamellar fine-structures increased with raising shock pressure. Therefore, these features could be used as shock pressure indicators while the estimated pressures may be lower limits due to no information of temperature dependence. For Martian meteorites that experienced heavy shocks, the minimum peak shock pressures of RBT 04261 and NWA 1950 are estimated to be 39.5–48.5 GPa and 48.5–56 GPa, respectively, which are found consistent with those estimated by postshock temperatures expected by the presence of brown olivine. We also investigated shock-recovered basalts preheated at 750 and 800 °C in order to check the temperature effects on shock features. The results indicate a reduction in vitrifying pressure of plagioclase and a pressure increase for PDFs formation in olivine. Further temperature-controlled shock recovery experiments will provide us better constraints to understand and to characterize various features found in natural shock events.

INTRODUCTION

Meteorites and their constituent minerals commonly exhibit various kinds of shock features such as shock melt veins, undulatory extinction, and amorphization. Such shock features have been used as indicators of shock events for the past several decades (e.g., Stöffler et al. 1991, 2018; Sharp and DeCarli 2006; Fritz et al.

2017). A formation of high-pressure minerals is one of the most useful shock features for estimating shock pressures in particular L chondrites and Martian meteorites (e.g., Miyahara et al. 2011; Greshake et al. 2013; Walton et al. 2014; Tomioka and Miyahara 2017; Ma 2018). However, shear stress can induce high-pressure phase transformation at lower pressure than equilibria (e.g., Mandon et al. 1989; Ji et al. 2012).

Moreover, the transformation pressure from phase equilibria can only provide the lower pressure bound of the shock because a high-pressure transformation is rate dependent and may take a longer time compared with typical shock durations of these meteorites: tens of milliseconds and several seconds for Martian meteorites and L chondrites, respectively (e.g., Ohtani et al. 2004; Beck et al. 2005; Walton et al. 2014). Due to such kinetic problems, most of high-pressure minerals are not confirmed in products of shock recovery experiments with significantly shorter shock durations (~microseconds) than those of meteorites. Hu and Sharp (2017) recently reported that a high-pressure phase of olivine (wadsleyite) in Mbale (L chondrite) was partly back-transformed to olivine due to short shock durations (<1 s) and high postshock temperature (~1200 K). Moreover, some Martian meteorites whose shock conditions were enough to form high-pressure minerals contain no high-pressure minerals because of back-transformation induced by short shock duration and high postshock temperatures (Walton 2013; Fritz et al. 2017; Takenouchi et al. 2017, 2018). In such meteorites, we could not estimate even lower limits of shock pressures. Therefore, we need to establish the other indicators for peak shock pressure estimation such as refractive indices of maskelynite (Milton and DeCarli 1963; Stöffler et al. 1986; Fritz et al. 2005).

In this study, we focused on planar deformation features (PDFs) of olivine. PDFs have been well studied in quartz and the term “planar deformation features” was defined by Grieve et al. (1990) to describe “optically recognizable, planar microstructures diagnostically produced in quartz by shock compression.” In contrast to high-pressure transformation, PDFs are considered to form immediately after the shock wave has passed (Goltrant et al. 1992; Fritz et al. 2017), and therefore, PDFs have the potential to retain the information of peak pressures (just after shock wave front or at two-wave structures by reflection on high-impedance phases) which is not recorded in high-pressure minerals. Goltrant et al. (1992) reported that there are four kinds of fine-structures in PDFs of quartz (1) bands of dislocations; (2) lamellae of mixtures of amorphous and crystalline silica; (3) twin lamellae; (4) short, parallel lamellae forming ladder structures. However, such fine-structures of PDFs were not reported enough in shocked olivine in meteorites (e.g., Müller and Hornemann 1969) although there are several studies focusing on hydrostatically formed dislocations in olivine (e.g., Phakey et al. 1972; Ashworth and Barber 1975). In the shock stage classifications by Fritz et al. (2017) and Stöffler et al. (2018), olivine PDFs have been considered to form when a shock pressure becomes over 45 GPa and 30–35 GPa, respectively. However, detailed observations of fine-

structures of PDFs in olivine are still required in order to precisely estimate shock pressures by using PDFs in olivine. Therefore, in this study, we performed shock recovery experiments of olivine and observed the fine-structures of PDFs in shocked olivine in order to establish an indicator of shock pressures. Furthermore, we compared the PDFs found in the recovered samples and in Martian meteorites to estimate their peak shock pressures.

METHODS AND SAMPLES

Shock recovery experiments were conducted using a single-stage propellant gun at the National Institute for Materials Science (NIMS), Tsukuba, Japan (e.g., Yamaguchi and Sekine 2000) (Fig. 1). The projectile (45 mm long and 30 mm in diameter) consists of polyethylene sabot and flyer plate of stainless (SUS 304, 3 mm in thickness) or tungsten (2 mm in thickness). Impact velocity was measured just before impact (Sekine 1997). Shock pressure in each shot is calculated based on the measured velocity using Hugoniot data for flyer and container (Marsh 1980). We used an SUS 304 container as described by Sekine (1997) (Fig. 1). In our experiments, six shots were performed aiming at pressures of 20–50 GPa. In two shots, samples were preheated about 800 °C, as described elsewhere (Sekine 1989). The Hugoniot parameter changes at high temperature, but there is no large difference (Duffy and Ahrens 1997). Here, we neglected the shift in calculating peak pressure. The peak shock pressure within sample was calculated assuming a pressure equilibrated with a container by reverberation due to thin sample relative to the flyer thickness. The reason why we performed the preheated shock experiments is below: the shock pressure in our shock recovery experiment was raised by shock wave reflection at the sample–container interface due to the differences in shock impedance of sample and containers (the shock reverberation technique). However, such a compression will generate lower shock heating compared to natural shock events where the pressure is raised by a single shock compression (e.g., Tomeoka et al. 1999). Therefore, in order to investigate temperature effects on shock metamorphism, preheated shock recovery experiments were conducted in addition to experiments at room temperature. According to calculations by Tomeoka et al. (1999), differences in waste heat energy after decompression between multiple shock wave reflections (experiments) and single-shock compression (planetary collisional event) are about 1570 and 2350 J g⁻¹ for 36.0 and 48.8 GPa, respectively. If such waste heat differences completely convert to a temperature, our

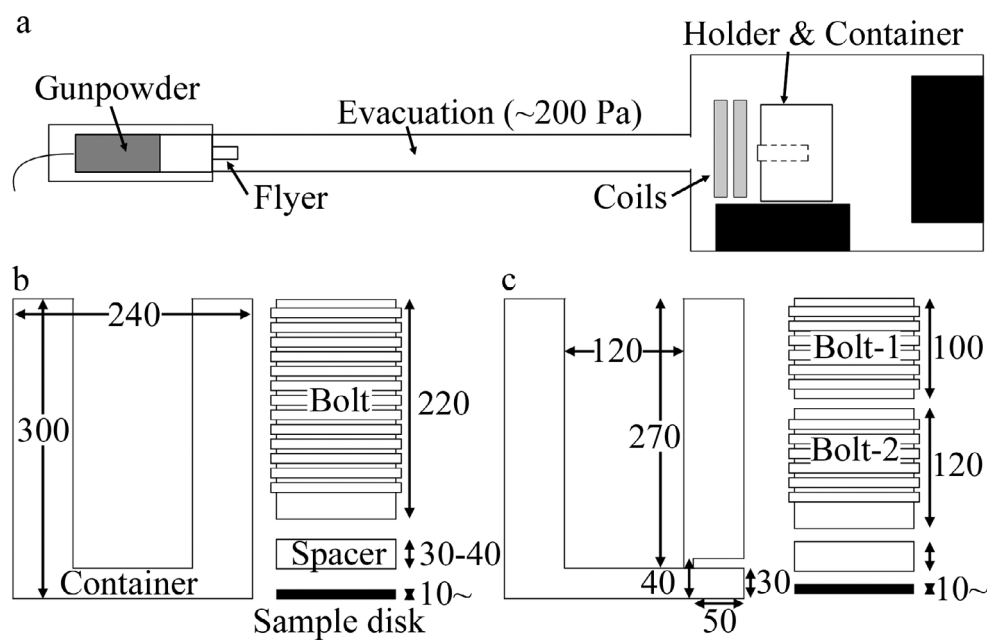


Fig. 1. A geometry of the single stage propellant gun we used (a) and schematic cross section images of sample container for shock recovery experiment at room temperature (b) and those with initial high temperature (c).

preheating temperature (750 and 800 °C) could not be enough to compensate for temperature differences described above. However, the preheated temperature of 800 °C is the upper limit in our heating system, and therefore, we adopted this temperature. Each experiment was performed under evacuated condition (~200 Pa) to shoot flyer straight without obstruction by the presence of air.

In our experiments, olivine-phyric basalt from Kita-Matsuura, Kyusyu, Japan, was selected as a target material. This basalt contains olivine phenocrysts (~3 mm) and its chemical composition (~Fo₆₉) is within the range of olivine composition of shergottites. The basalt rocks were cut as circular disks of about 1 mm thick with 12 mm diameter. The sample disk is settled in the bottom of the container pit and tightly sealed by a stainless screw bolt after inserting a spacer for a height adjustment. The preheating system was prepared for each shot because the system is broken every time. In one experiment, the Kanthal wire was snapped during heating and the temperature could not reach 800 °C, and therefore, the sample was shocked at 750 °C. In the same experiment, the velocity of projectile could not be measured but was estimated based on the propellant amount (see Table 1). The recovered samples were roughly cut open by a lathe and sliced by a diamond cutter at NIMS, and then, thin sections were made at the University of Tokyo. Shock pressures were 22.2, 28.7, 39.5, and 48.5 GPa at room temperature sample and ~22.2 and ~39 GPa for high temperature samples (Table 1).

For comparison with the recovered samples, we prepared two Martian meteorites, Northwest Africa (NWA) 1950 and Robert Massif (RBT) 04261. Both meteorites are poikilitic shergottites and contain maskelynite (e.g., Usui et al. 2010; Takenouchi et al. 2017, 2018) indicating that they were subjected to high pressures at least >25–35 GPa (e.g., Fritz et al. 2017). NWA 1950 is known to contain brown-colored olivine (brown olivine) but no high-pressure minerals (Takenouchi et al. 2017). RBT 04261 contains small amounts of high-pressure minerals but almost no brown olivine (Takenouchi et al. 2018). We investigated thick sections of olivine grains for both meteorites.

Polished thick and thin sections of the shock recovered samples and Martian meteorites were first observed by a field emission scanning electron microscopy (FE-SEM: JEOL JSM-7100F) at the National Institute of Polar Research, Tokyo (NIPR). Electron backscattered diffraction (EBSD) analysis was also performed by the SEM for crystal orientation analysis of olivine. Obtained Kikuchi patterns were compared with simulated ones from forsterite (space group: *Pnma*) using Aztec 3.0 developed by Oxford Instruments. Quantitative chemical analyses were performed by a field emission electron microprobe (JEOL JXA-8530F) at the University of Tokyo. Analytical conditions for quantitative analysis of olivine and pyroxene were 20 kV in accelerating voltage, 20 nA in beam current, and 1 μm in beam diameters. Those for plagioclase (maskelynite) were 15 kV, 8 nA, and 5 μm, respectively, in order not to lose volatile elements

Table 1. Summary of our observations of basalts recovered at six shock conditions.

Projectile's velocities	Estimated peak pressure (GPa) ^a	Initial temperature	Olivine	Plagioclase	Whole rock
1.05 km s ⁻¹	22.2	Room temperature	Undulatory extinction Planar fractures	Undulatory extinction Crystalline	
1.31 km s ⁻¹	28.7	Room temperature	Undulatory extinction Planar fractures	Maskelynitization Less cracks	Shock melt veins at fractures
1.71 km s ⁻¹	39.5	Room temperature	Undulatory extinction Planar fractures Defect-rich lamellar textures	Maskelynitization	Shock melt veins
1.57 km s ^{-1b}	48.5	Room temperature	Undulatory extinction Planar fractures Defect-rich lamellar textures	Maskelynitization Ambiguous zoning in composition	Shock melt veins
1.05 km s ⁻¹	~22.2	800 °C	Undulatory extinction Planar fractures	Undulatory extinction Partial maskelynitization	Shock melt pockets at grain boundaries
~1.7 km s ^{-1c}	~39	750 °C ^d	Undulatory extinction Planar fractures	Maskelynitization Flow textures (melting)	Abundant voids Shock melt pockets and veins

^aCalculated by shock impedance matching in the case of stainless–stainless collision.

^bUsing not a stainless steel flyer but a tungsten flyer.

^cVelocity based on the amount of gun powder because the oscilloscope for measuring the velocity was down after shots due to blackout induced by the heating system.

^dThe Kanthal wire was snapped during heating before the temperature reached 800 °C.

in particular Na due to a high beam current. Elemental maps were also obtained by the microprobe under the conditions of 20 kV for accelerating voltage and 70 nA for beam current. The areas with fine-textures observed in the samples were cut by focused ion beam (FIB: Hitachi FB-2100, gallium ion source with 30 and 10 kV) and observed by transmission electron microscopy (TEM: JEOL JEM 2010, accelerating voltage: 200 kV) both at the University of Tokyo.

OBSERVATION RESULTS

Olivine in Unshocked Basalt

The basalt used in the present experiments contains phenocrysts of olivine, pyroxene, and plagioclase (Fig. 2). The size of each phenocryst is about 500 µm. The matrix is composed of plagioclase lath, clinopyroxene, cristobalite, phosphate, and opaque minerals. The plagioclase lath is up to 500 µm in length and the other fine-grained minerals are less than 100 µm in size. Due to their small sizes, observation of matrix minerals by optical microscopy was difficult and insufficient. BSE image shows that olivine has reaction rims of orthopyroxene and ilmenite. Quantitative chemical compositions are shown in Fig. 3 and Table 2. The compositions of the olivine phenocrysts are Fo_{68.7-71.6}, close to those in Martian meteorites.

The olivine phenocryst contains reddish- to brownish-colored areas under plane polarized light (Fig. 2a). In SEM observation, such colored areas could be recognized as brighter and rough surface areas within olivine (Fig. 2c). These observations indicate that olivine phenocrysts in this basalt have been slightly altered, and therefore, a careful interpretation is needed when we investigate the shock effects in the recovered sample.

Basalt Shocked at Room Temperature

The shocked basalt sample at 22.2 GPa indicates undulatory extinction of plagioclase, pyroxene, and olivine under an optical microscope (Figs. 4a and 4b) and is severely fractured while shock melt veins were rarely observed. All constituent minerals have irregular cracks and olivine shows small amounts of planar fractures (Figs. 4c and 4d).

In contrast to the basalt shocked at 22.2 GPa, plagioclase in the basalt shocked at 28.7 GPa was completely maskelynitized and showed less abundant cracks (Fig. 5). BSE observation clarified that plagioclase (maskelynite) still retained a compositional chemical zoning (Fig. 5c). Shock-induced melt (fractured) veins were commonly observed in the basalt shocked at 28.7 GPa (Fig. 5d). However, olivine and pyroxene in this recovered sample (shocked at

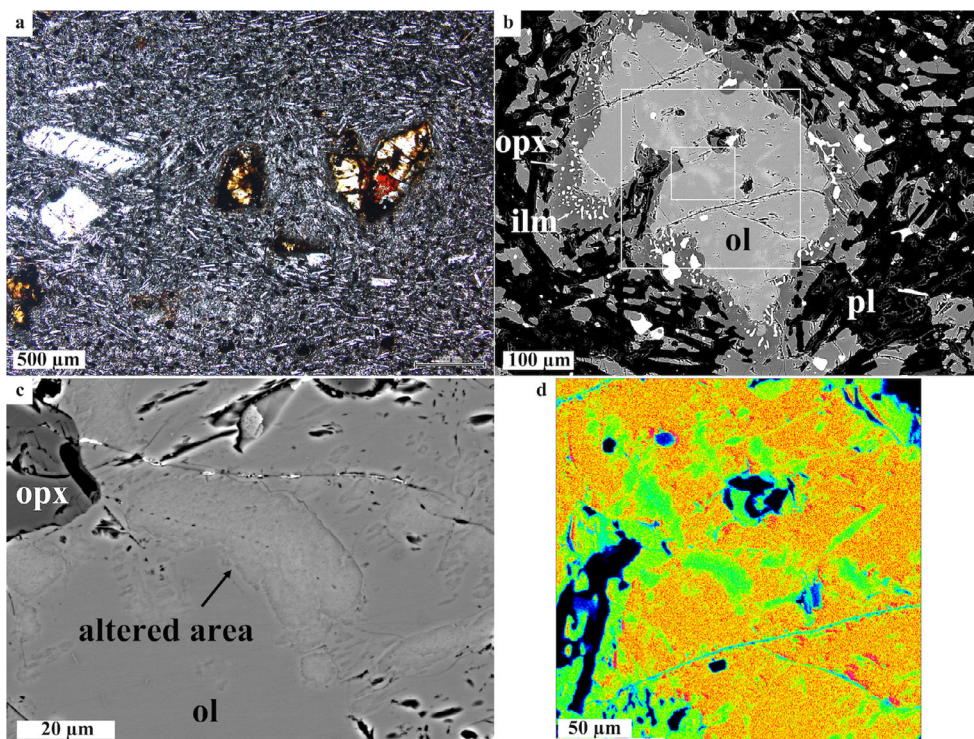


Fig. 2. Plane polarized light (PPL) image (a), BSE images (b, c), and X-ray chemical map (Mg) of intact (unshocked) basalt and olivine (d). Small and large white squares in (b) represent the areas shown in (c) and (d), respectively (ol = olivine, opx = orthopyroxene, ilm = ilmenite, pl = plagioclase). (Color figure can be viewed at wileyonlinelibrary.com.)

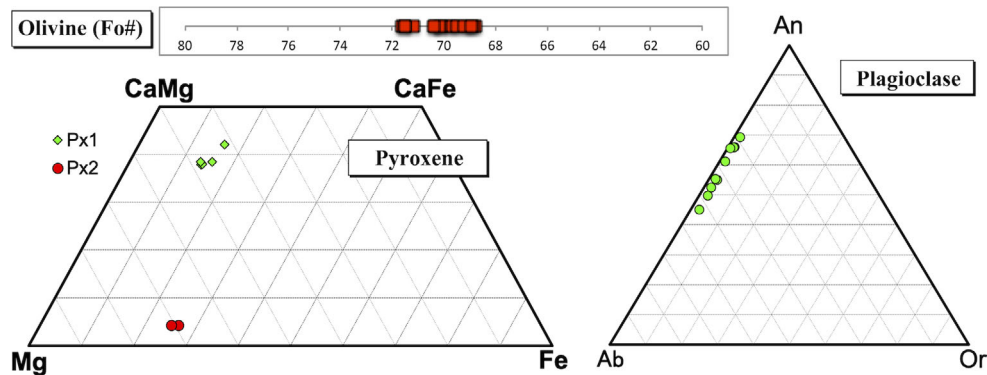


Fig. 3. Chemical compositions of minerals in intact basalt. Clinopyroxene is a phenocrystal grain and orthopyroxene is a reaction rim of olivine. The chemical compositions range $\text{En}_{41.6}\text{Wo}_{42.1}\text{-En}_{48.2}\text{Wo}_{37.9}$ and $\text{An}_{45.1}\text{Ab}_{52.6}\text{-An}_{69.3}\text{Ab}_{29.1}$ for clinopyroxene and plagioclase, respectively ($\text{Fo}\# = \text{Mg}/[\text{Mg} + \text{Fe}]$, An = anorthite, Ab = albite, and Or = orthoclase). (Color figure can be viewed at wileyonlinelibrary.com.)

Table 2. Chemical compositions of minerals in the basalt used in the present study.

Phase	SiO ₂	Al ₂ O ₃	TiO ₂	FeO	MnO	MgO	CaO	Na ₂ O	K ₂ O	Cr ₂ O ₃	NiO	Total	<i>N</i>
Olivine	36.8	0.02	0.02	27.11	0.44	35.72	0.1	n.d.		0.03	0.14	100.39	17
Orthopyroxene	52.66	0.8	0.51	16.66	0.39	25.42	2.14	0.02		0.04	0.04	98.68	2
Clinopyroxene	51.39	1.83	0.54	9.2	0.26	16.2	18.96	0.31		0.22	0.02	98.93	5
Plagioclase	52.61	28.41	0.1	0.86	0.01	0.05	11.89	4.46	0.3		0.03	98.72	10

n.d. = not detected.

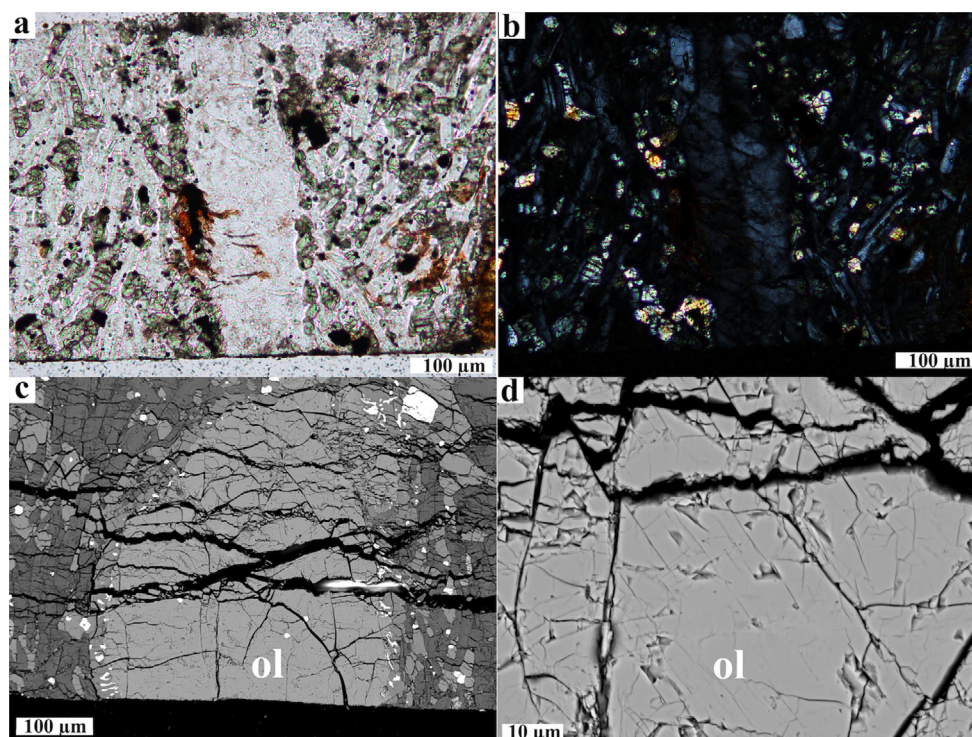


Fig. 4. PPL image (a), crossed polarized light (CPL) image (b), and BSE images (c, d) of basalt and olivine shocked at 22.2 GPa. Plagioclase shows undulatory extinction (not maskelynite) (b) and olivine shows planar fractures (d) (ol: olivine). (Color figure can be viewed at wileyonlinelibrary.com.)

28.7 GPa) show only undulatory extinction and abundant cracks, and no other significant shock features were observed.

Basalt samples recovered from shock pressure of 39.5 GPa (Fig. 6a) and 48.5 GPa (Fig. 7a) show the maskelynitization of plagioclase and the chemical zoning of maskelynite is deformed compared with intact plagioclase before shock. The grain boundaries between plagioclase and silica glasses were curving due to the shock compression. Microfaults commonly cut across each mineral obliquely accompanied by shock melt veins throughout the sample (Figs. 7b and 7c). While pyroxene shows only undulatory extinction, olivine phenocrysts in the basalt shocked at 39.5 and 48.5 GPa show distinct features from those of olivine shocked below 28.7 GPa. In the basalt shocked at 39.5 GPa, planar fractures are dominant in olivine (Figs. 6b and 6c) and some parts of olivine show ladder-like lamellar textures (Fig. 6d). Olivine shocked at 48.5 GPa also shows the lamellar textures (Fig. 7d). Since these lamellae were not observed in the intact olivine, these lamellar textures were formed by shock metamorphism. The maximum widths of the lamellae are ~ 0.25 and ~ 1 μm in olivine shocked at 39.5 and 48.5 GPa, respectively. The lamellae became thicker and more abundant as the shock pressure increased although

lamellar lengths were not significantly changed in our experiments (Fig. 8). For further investigations, the lamella in the shock pressure of 48.5 GPa was cut off perpendicular to its elongated orientation by FIB to observe by TEM (Fig. 9a).

TEM observation revealed that olivine in the basalt shocked at 48.5 GPa has abundant defects. There is an area composed of defects forming a streak across the FIB section (Fig. 9b). This streak is 230 nm thick and we could not define crystallographic orientation in this section. There are no other characteristic features in this FIB section; therefore, the streak may represent the lamellar texture observed in SEM observation. In other words, the lamellar textures are composed of abundant defects formed in the shocked olivine.

Basalt Shocked at Higher Temperatures

Observations by SEM clarified that both preheated shock recovered samples (shocked ~ 22.2 GPa at 800 $^{\circ}\text{C}$ and ~ 39 GPa at 750 $^{\circ}\text{C}$) had shock melt pockets at grain boundaries between plagioclase, silica glass, and pyroxene. The basalt sample shocked ~ 39 GPa at 750 $^{\circ}\text{C}$ had abundant voids (~ 10 μm in diameter) in the melt pockets throughout the sample. In the recovered sample shocked ~ 22.2 GPa at 800 $^{\circ}\text{C}$, plagioclase was mostly

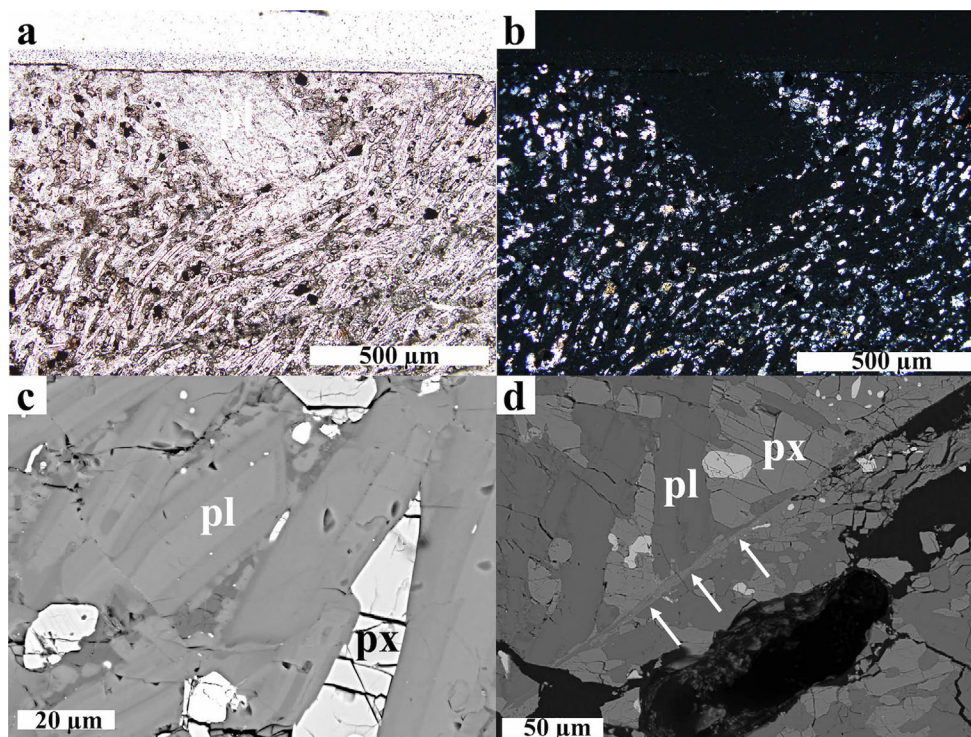


Fig. 5. PPL (a), CPL (b), and BSE (c, d) images of basalt shocked at 28.7 GPa. Plagioclases are completely converted to maskelynite (a, b) while maskelynite retains chemical compositional zoning (c). White arrows in (d) indicate a shock-induced melt vein (pl = plagioclase, px = pyroxene). (Color figure can be viewed at wileyonlinelibrary.com.)

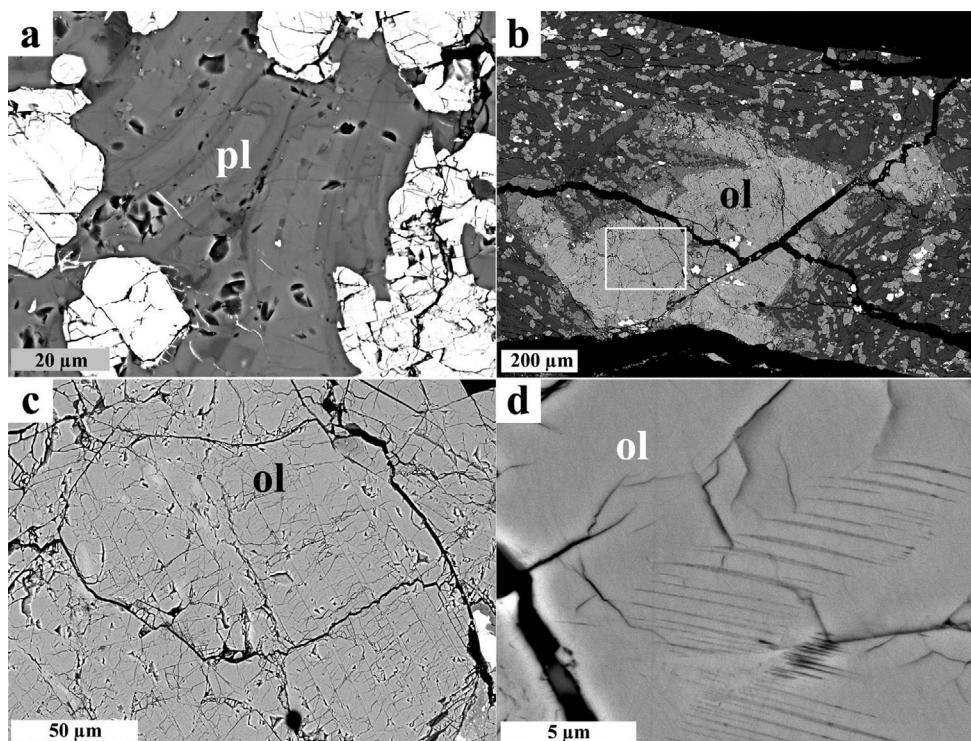


Fig. 6. BSE images of the basalt sample shocked at 38.5 GPa. Plagioclase (maskelynite) shows deformed chemical compositional zoning (a). Olivine shows planar fractures (b, c) and lamellar texture (d) (ol = olivine, pl = plagioclase).

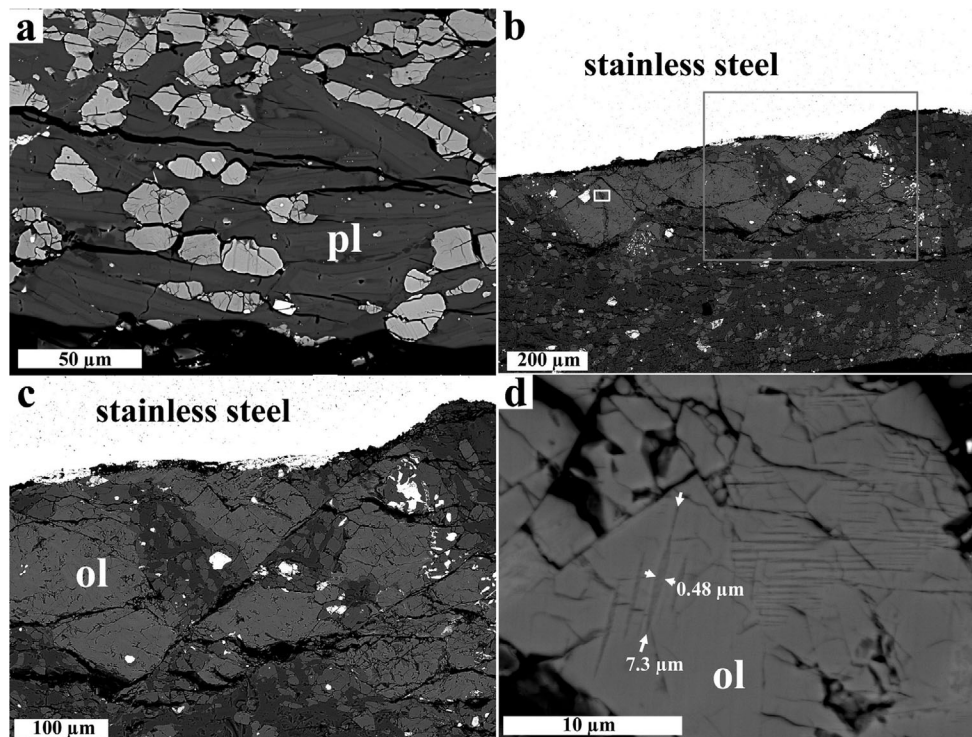


Fig. 7. BSE images of the basalt sample shocked at 48.5 GPa. Plagioclase shows a compressed shape and its chemical zoning was deformed along grain boundaries (a). Microfaults were often observed (b, c) and olivine has a lamellar texture (d) similar to those in Fig. 6d. White arrows in (d) display the length and width of one lamella as 7.3 and 0.48 μm , respectively (ol = olivine, pl = plagioclase).

isotropic (maskelynitized) while part of plagioclase showed a little undulatory extinction under crossed polarized light (CPL) (Figs. 10a and 10b). Plagioclase shocked ~ 39 GPa at 750°C was maskelynitized and bending with flow textures (Figs. 11a and 11b). Although the chemical zoning of plagioclase shocked ~ 22.2 GPa at 800°C is well retained (Fig. 10c), melting of sodic rims and shock compression disturbed the chemical zoning in plagioclase shocked ~ 39 GPa at 750°C and the grain boundaries are not straight compared with the original texture (Figs. 11a and 11b). Pyroxene shows undulatory extinction and abundant cracks indicating that there was almost no difference between pyroxene in samples shocked at high temperature and those shocked at room temperatures.

Olivine shocked at high temperature shows undulatory extinction under CPL and shows clear planar fractures similar to those shocked at room temperature (Fig. 10d). SEM observation showed that there were brighter BSE contrast areas within olivine grains (Figs. 10d, 11c, and 11d). However, the brighter areas represent initially altered and then annealed (probably dehydrated) areas by heating before shock loading indicating no shock features. The lamellar textures found in the olivine shocked at 38.5 and 48.5 GPa at room temperature (Figs. 6d and 7d) were

not found in the recovered samples from ~ 39 GPa at high temperatures ($\sim 750^\circ\text{C}$).

Martian Meteorites

Olivine in NWA 1950 is darkened throughout the meteorite and such olivine is called “brown olivine” (e.g., Takenouchi et al. 2017; Treiman et al. 2007). Olivine in RBT 04261 is colorless while olivine just around shock melt veins is locally darkened (Takenouchi et al. 2018). While detailed description of “brown olivine” in these meteorites is found in Takenouchi et al. (2018), this study performed detailed SEM observation of “colorless” olivine in both meteorites.

Olivine in both meteorites showed undulatory or mosaic extinction under CPL as is the case of severely shocked olivine. SEM observation of olivine in both meteorites revealed the presence of lamellar textures (Fig. 12). They were not found in brown olivine but observed in the experimentally shocked basalt at 39.5 and 48.5 GPa at room temperature (Figs. 6 and 7). The lamellae were much abundant in NWA 1950 while it was rare in RBT 04261 (Fig. 8). The apparent maximum widths of lamellae in NWA 1950 and RBT 04261 were about 1.1 and 0.5 μm , respectively. The mode width and

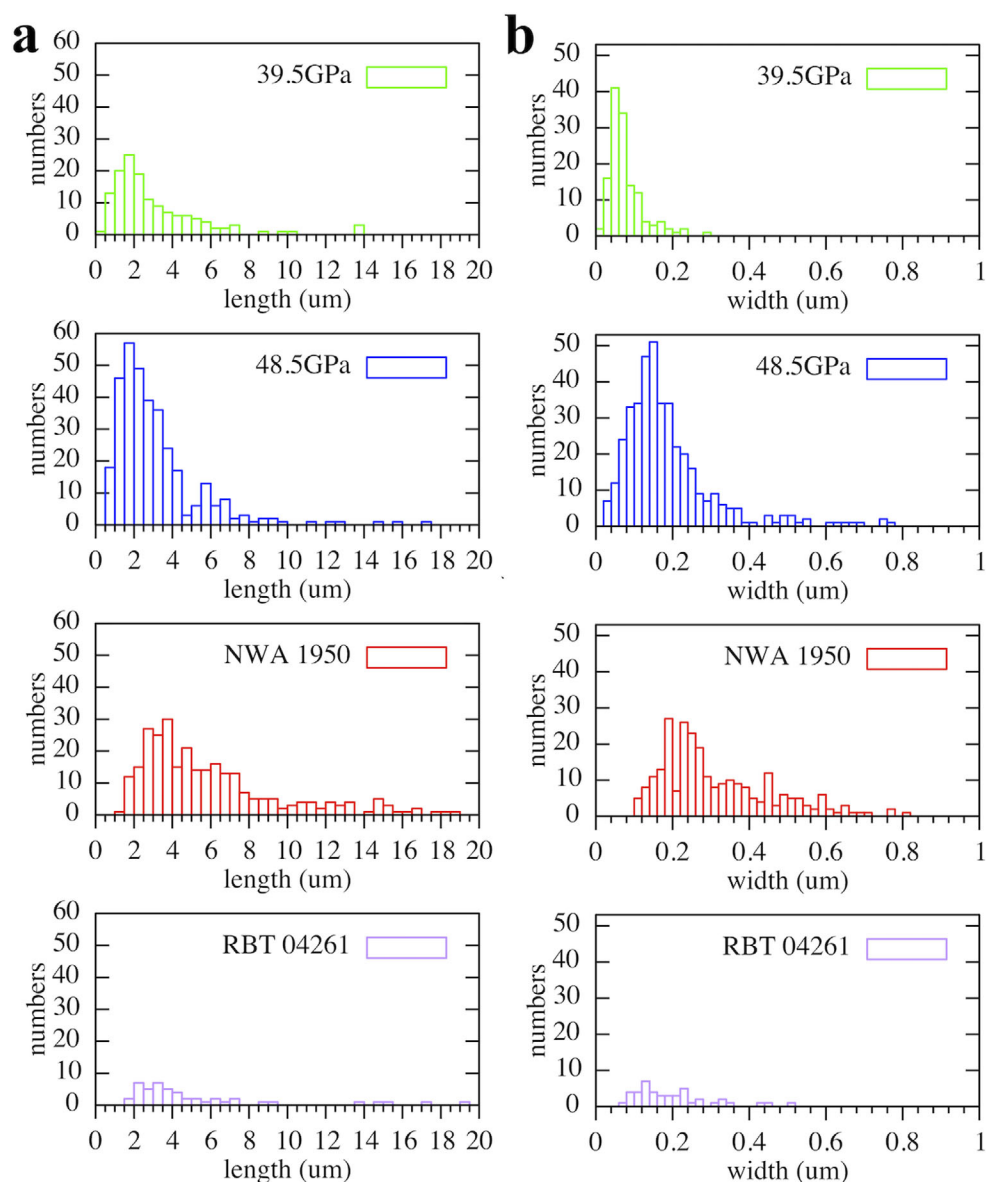


Fig. 8. Histograms of lamella length (a) and width (b) in shock experiments and Martian meteorites. While mode values of lamellar length are almost the same between two shock experiments, those of lamellar width became higher as shock pressure increased. The lamellar width mode value in NWA 1950 is higher than those of our experiments and RBT 04261. (Color figure can be viewed at wileyonlinelibrary.com.)

length of the lamellae in NWA 1950 were thicker and longer than our experimental results (Fig. 8). The lamellae had darker contrast in BSE images compared to the surrounding olivine crystal and they were parallel to a few crystallographic orientations of olivine such as $\{021\}$ by EBSD analysis (Fig. 12b). In order to observe these lamellae in detail, FIB sections were made perpendicular to the lamellar elongated directions to observe by TEM.

TEM observation of the FIB sections revealed that the olivine lamellae in NWA 1950 showed smooth appearance rather than a streak of defects (Fig. 13). The host olivine around the lamellae contains a small

number of dislocations ($[001]_{\text{host olivine}}$) compared with the area far from lamellae. TEM-EDS analyses of the lamellae and host olivine exhibited no compositional differences between them (Fig. 13). Electron diffraction patterns clarified that the lamellae are amorphous and develop parallel to $(0\bar{2}1)_{\text{host olivine}}$. The lamellar textures found in RBT 04261 are not amorphous but composed of abundant defects akin to those observed in experimentally shocked samples (Figs. 9 and 14). These observations indicate that there are at least two kinds of fine-structures in shock-induced olivine lamellae.

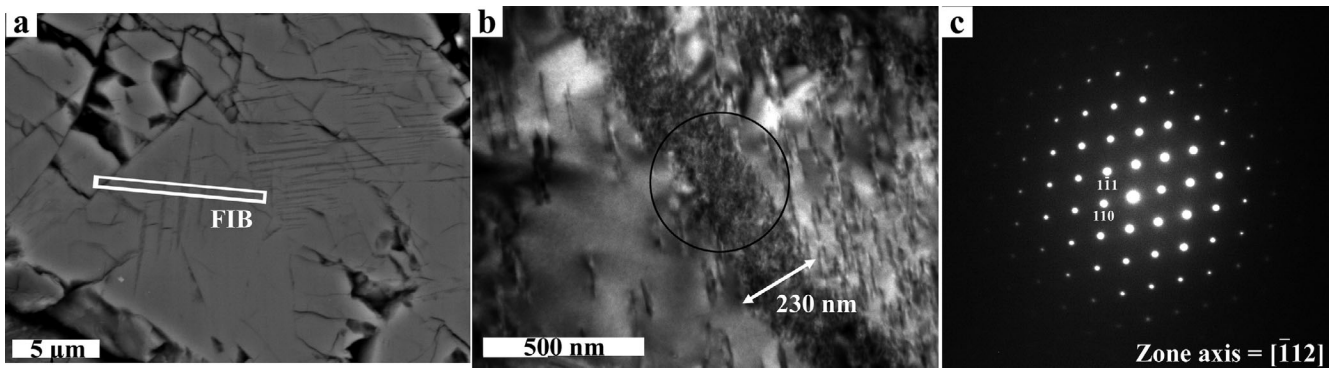


Fig. 9. BSE image (a) of lamella in olivine shocked at 48.5 GPa with FIB section area indicated by a white rectangle. TEM bright-field (BF) image (b) of lamella in the FIB section. Lamellar areas observed in (a) were composed of abundant defects (b). We cannot determine any crystallographic orientations of this lamella from a selected area (SA) diffraction pattern (c) obtained from the area shown by a black circle in (b).

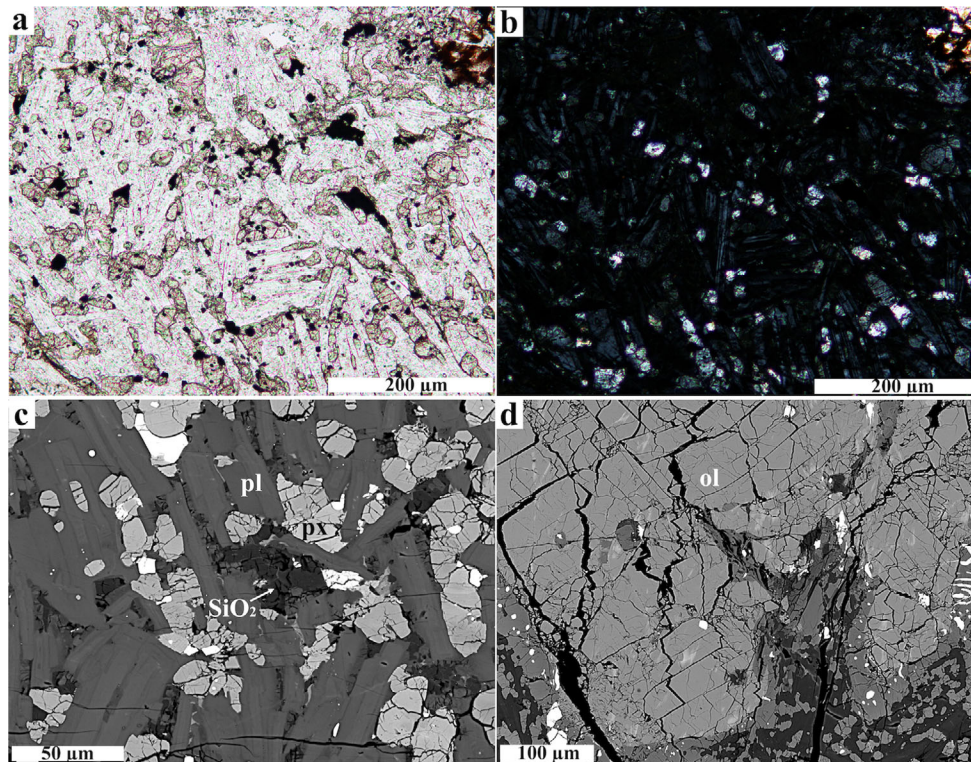


Fig. 10. PPL (a), CPL (b), and BSE (c, d) images of basalt shocked ~ 22.2 GPa at 800 °C. Almost all plagioclase was maskelynitized (a, b) while maskelynite still shows sharp chemical compositional zoning (c). Olivine shows clear planar fractures although we cannot define its crystallographic orientations now (ol = olivine, px = pyroxene, pl = plagioclase). (Color figure can be viewed at wileyonlinelibrary.com.)

DISCUSSION

Shock Features in Shock-Recovered Minerals and Comparison with Previous Studies

In the previous shock recovery experiments on olivine, single crystal and polycrystal were used for

investigation of shock-induced features in olivine (e.g., Bauer 1979; Syono et al. 1981; Farrell-Turner et al. 2005). Chondritic meteorites were also adopted for target materials in order to investigate the shock features in ordinary and carbonaceous chondrites (e.g., Tomeoka et al. 1999; Schmitt 2000). Yamaguchi and Sekine (2000) used a plagioclase disk in contact with

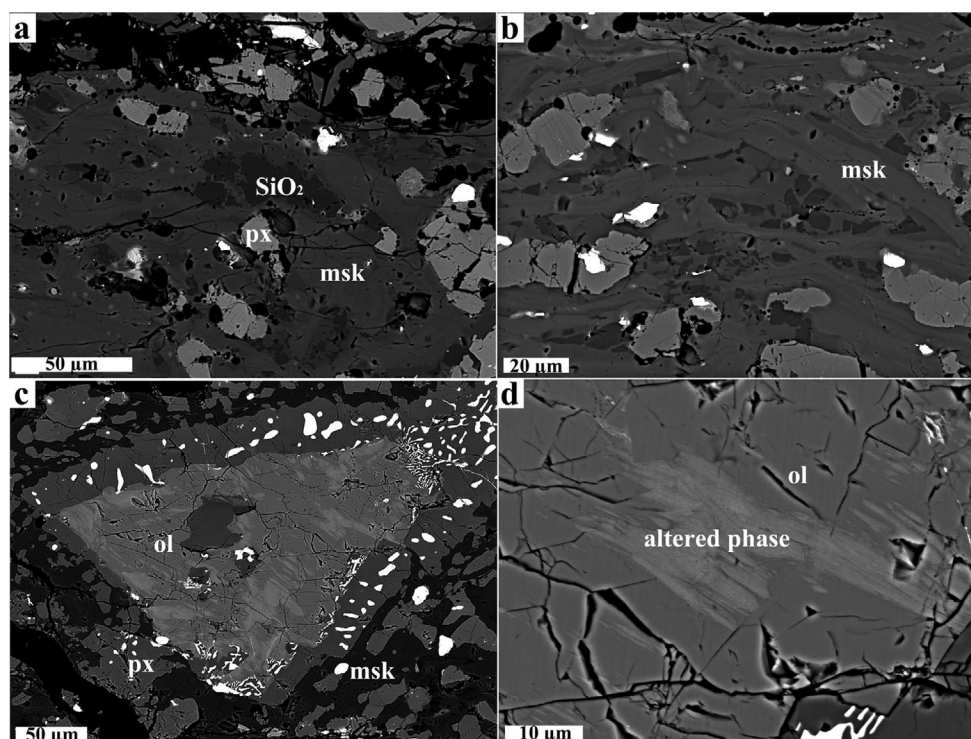


Fig. 11. BSE images of basalt shocked ~ 39 GPa at 750 °C. Grain boundaries between maskelynite and SiO_2 -glass are ambiguous due to partial melting at boundaries (a). Chemical compositional zoning in maskelynite is highly disturbed by partial melting and shock compression (b). Olivine shows brighter contrast derived from altered phase while we cannot find lamellar structures (c, d).

pyroxene disk as target materials for shock recovery experiments in order to investigate a behavior of amorphous plagioclase under shock events. Recently, Stöffler et al. (2018) summarized the results of shock recovery experiments to revise shock stage classifications for several target materials based on their shock textures. Due to the differences in initial textures of target materials, the shock features should be different in each material. Therefore, our shock recovery experiments on an olivine-phyric basalt provide shock features and corresponding shock pressures for each mineral in some Martian meteorites.

Plagioclase

Our experiments shocked at 22.2 and 28.7 GPa indicate that the maskelynitization pressure of plagioclase ($\text{An}_{45-69}\text{Or}_{-2}$) in basalt ranges between 22.2 and 28.7 GPa in the shock recovery experiments at room temperature, which is almost consistent with those reported previously (e.g., Stöffler et al. 1986; Fritz et al. 2005).

Pyroxene

Due to small sizes of pyroxene, we cannot determine detailed characteristic shock features in pyroxene. Therefore, our sample was not suitable and

different sample should be prepared for determining the shock features of pyroxene.

Olivine

Olivine shocked below 28.7 GPa only shows well-documented shock features such as undulatory extinction and planar fractures (e.g., Reimold and Stöffler 1978; Bauer 1979; Fritz et al. 2017; Stöffler et al. 2018). The most remarkable shock feature in our experiments is ladder-like lamellar texture observed by SEM (Figs. 6d and 7d). Such textures were observed in room temperature olivine shocked at 39.5 and 48.5 GPa. Their ladder-like shape indicates their shear deformation origin in the same analog as en echelon fractures (e.g., Cloos 1955). Since the lamellae were not recognizable under optical microscopy probably due to the small sizes and high refractive index of host olivine, they are not matched with the definition of PDFs of olivine by Grieve et al. (1990). However, we call these lamellar textures PDFs because the lamellae are planar and formed by deformation.

The duration of such PDFs's formation must be shorter than $1 \mu\text{s}$ because they were induced by shock wave propagation in our shock recovery experiment. Therefore, instead of high-pressure minerals, features of such lamellae may represent the information of peak

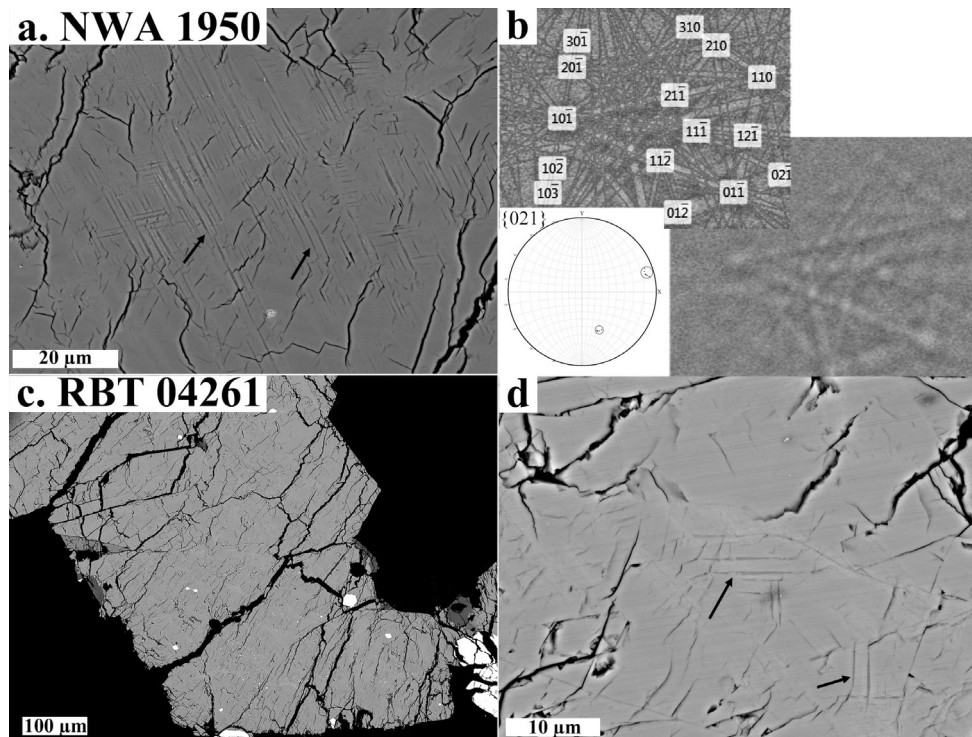


Fig. 12. BSE image of olivine lamellae in NWA 1950 (a), Kikuchi patterns obtained from the host olivine, simulated ones, polar plots of $\{021\}$ of host olivine (b), and BSE images of olivine in RBT 04261 (c, d). Black arrows in (a, d) represent lamellar textures in NWA 1950 and RBT 04261, respectively.

shock pressure. In our shock experiments, both the lamellar width and number density of lamellae increased with increasing shock pressure (Fig. 8). Therefore, these factors may be useful indicators to estimate peak shock pressure. We will discuss details in the following section.

Shock Features in Preheated Basalt

Our experimental results on preheated basalt revealed slightly different shock features compared with those at room temperature. The absence/presence of maskelynite in samples shocked at 22.2 GPa with room temperature and initial high temperature (800 °C) indicates that high initial temperature lowers shock pressures essential for maskelynitization (Figs. 4 and 10), which is consistent with the results by static high-pressure and high-temperature experiments (Kubo et al. 2010) and preheated shock experiments using granite and eucrites (e.g., Huffman et al. 1993; Yamaguchi et al. 2003). Then, we infer that the minimum shock pressure for maskelynitization in natural shock events must be lower than those in shock recovery experiments at room temperature because the peak temperatures of natural shock events are higher than those by experiments due to the different compressions (single shock compression or reverberation shock). In order to

precisely estimate the essential pressure for maskelynitization by shock recovery experiments, we need to equalize the peak shock temperature between experimental and natural shock events at a shock pressure by adjusting the initial temperature in experiments. Regarding olivine shock features, PDFs observed in the basalt shocked at 39.5 and 48.5 GPa at room temperature (Figs. 6 and 7) were not observed in the sample shocked ~ 39 GPa with initial temperature 750 °C. One of reasons why PDFs were not observed might be that the formation of PDFs may have a little temperature dependence and the peak shock pressure (~ 39 GPa) of preheated experiments could not reach enough pressure to induce a significant number of PDFs under high-temperature condition. Therefore, PDFs' formation in meteoritical olivine indicates peak shock pressure at least >39.5 GPa, which is close to the pressure estimation (>45 GPa) suggested by Fritz et al. (2017). Since deformation features can change by temperature even under the same shock pressures, we need to pay more attention not only to shock pressure and duration but also to shock temperature when we compare shock features in samples between shock recovery experiments and natural impact events.

This study revealed that preheated shock recovery experiments would lead to different results from those

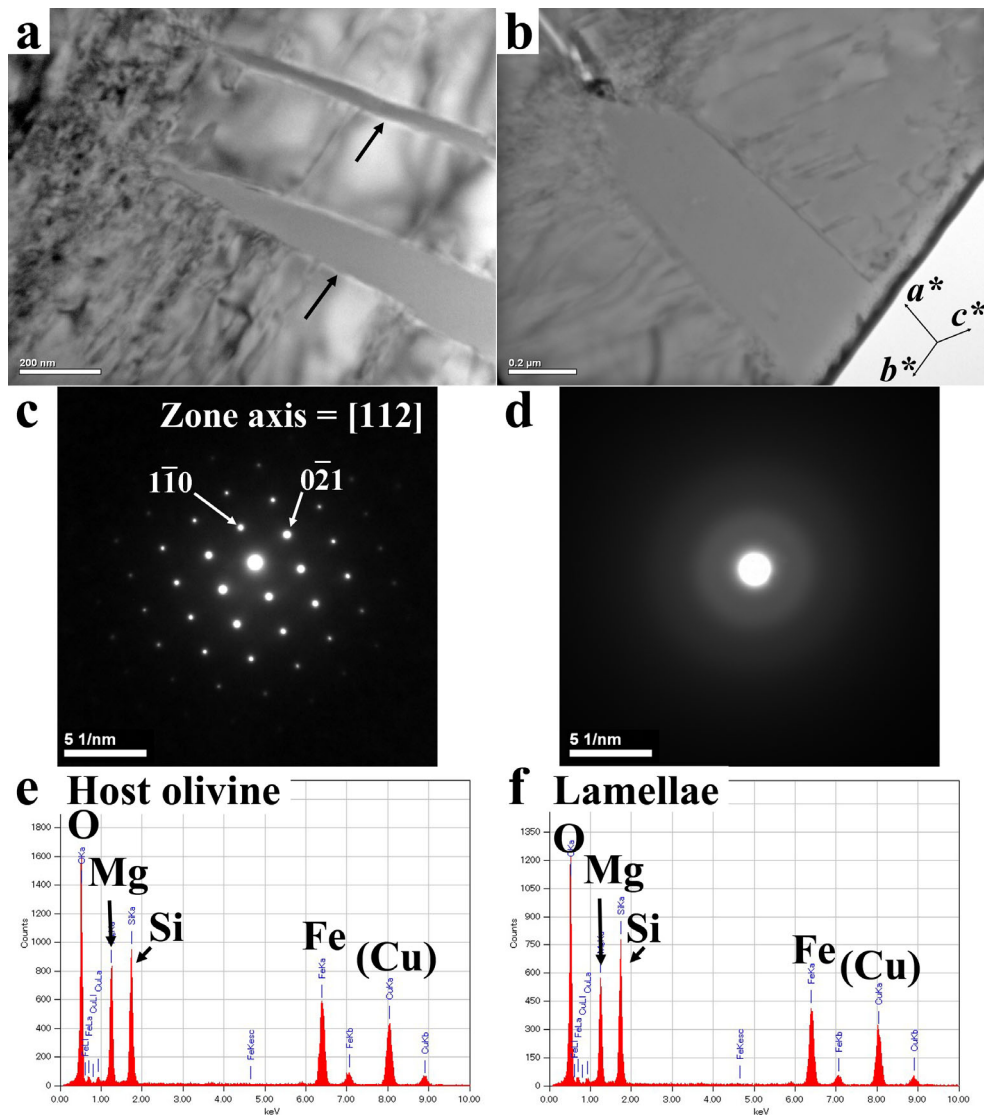


Fig. 13. TEM-BF images of olivine in NWA 1950 (a, b), SA diffraction patterns obtained from the host olivine (c) and lamellae (d), TEM-EDS spectra of the host olivine (e) and lamellae (f). Cu is derived from sample grids. Black arrows indicate lamellar textures representing those observed in SEM observations. (Color figure can be viewed at wileyonlinelibrary.com.)

at room temperature such as lowering vitrified pressure in plagioclase. Combining with static high-pressure experiments, temperature-controlled shock recovery experiments will provide better constraints on relations between shock pressures and corresponding features in natural shock events because the time scale of natural collision is at intermediate range between shock recovery experiments and static experiments.

Shock Features of Olivine in Martian Meteorites and Pressure Estimations

Olivine experimentally shocked at 39.5 and 48.5 GPa showed PDFs composed of defects (Figs. 6, 7,

and 9) and olivine in RBT 04261 showed similar textures to the PDFs (Fig. 14). PDFs observed in olivine of NWA 1950 were without defects and composed of amorphous olivine whose chemical composition is identical to that of the host olivine (Fig. 13). In our experiments on basalt at room temperature, the lamellar width and number density of PDFs became larger as the shock pressure increased (Fig. 8) whereas the shock duration was not so different between shock at 39.5 GPa with stainless steel flyer (1.71 km s^{-1}) and shock at 48.5 GPa with tungsten flyer (1.57 km s^{-1}). This trend indicates that the lamellar width and the number density mainly depended on peak shock pressures but not shock durations. This

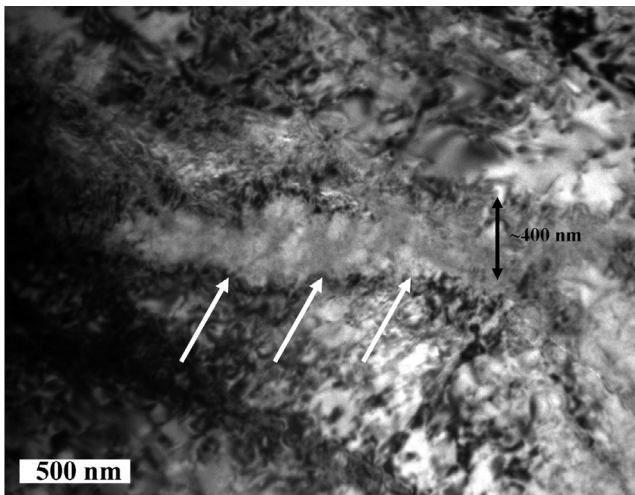


Fig. 14. TEM-BF images of olivine in RBT 04261. Lamellae observed in BSE images were corresponding to defects indicated by white arrows.

explanation is similar to “destructive shock effects” suggested by Fritz et al. (2017) that they are represented by the physical manifestation of the pressure–volume work achieved by the shock wave. Then, we can estimate peak shock pressures based on the lamellar width and number density although the estimated pressure in this way is possibly lower due to lack of temperature effects consideration. Comparing the lamellar width and number densities of PDFs between experimental samples and Martian meteorites, mode of lamellar width in RBT 04261 (0.12–0.14 μm) is within those in two experimental samples (0.04–0.06 and 0.14–0.16 μm for 39.5 and 48.5 GPa, respectively). The number density of PDFs in RBT 04261 is qualitatively close or lower to those of experimental samples shocked at 39.5 GPa. These observations suggest a peak shock pressure of RBT 04261 between 39.5 and 48.5 GPa. The lamellar width mode of $\sim 0.2 \mu\text{m}$ and the high number density in NWA 1950 may give a peak shock pressure of NWA 1950 higher than 48.5 GPa. Moreover, the most different feature is that the textures of PDFs in NWA 1950 were amorphous while those in RBT 04261 and experimental samples were composed of defects. Since there were no chemical compositional differences between the amorphous lamellae and the host olivine, the amorphous lamellae should have been formed without melting similar to amorphization of some plagioclase. Amorphization of olivine has been previously reported in shock recovery experiments (Jeanloz et al. 1977; Jeanloz 1980) and static compression experiments (e.g., Santamaria-Perez et al. 2016). In the shock recovery experiment using a single olivine crystal performed by Jeanloz et al. (1977),

olivine exhibited local amorphous area at a shock pressure of 56 GPa, although Jeanloz (1980) reported that this amorphization may be induced by localized intense strain, and therefore, pressure for olivine amorphization is around 56 GPa. Our experiments are consistent with those experimental results because olivine amorphization is not observed in our shock recovery experiments by a shock pressure of 48.5 GPa which is lower than those of the previous experiments. Santamaria-Perez et al. (2016) reported that pressure-induced amorphization started near 41 GPa and completed by 54 GPa under static conditions. However, olivine amorphization in Santamaria-Perez et al. (2016) is certified only by Raman analysis during compression and its texture is unclear. The texture of the amorphous area in NWA 1950 is rather similar to those observed in olivine shocked at 56 GPa (Jeanloz et al. 1977) except for the surrounding host olivine. The surrounding host olivine in the previous experiments contained abundant defects or dislocations while such defects were not so abundant around the PDFs in NWA 1950 (Fig. 13). One possible explanation for the absence of defects around amorphous areas in meteorite samples is due to postshock heating. As mentioned above, shock recovery experiments induce lower post shock temperature compared with natural shock event in particular at higher shock pressure. Lower postshock temperature in the experiments preserves abundant defects induced by the propagation of shock waves while high postshock temperature in Martian meteorites annealed the defects around amorphous areas. In fact, Takenouchi et al. (2017, 2018) reported that postshock heating of NWA 1950 was at least $>900 \text{ }^\circ\text{C}$, which could partly anneal these defects (Goetze and Kohlstedt 1973). Our TEM observation also suggests the dissolution of defects into amorphous areas because dislocations around amorphous areas were connected to amorphous areas while dislocations were abundant far from amorphous areas. Therefore, the amorphous lamellae observed in NWA 1950 olivine may have an identical formation process to that of amorphous lamellae reported by Jeanloz et al. (1977); amorphous areas formed at the highest strain area with abundant defects while the surrounding defects were healed after decompression by postshock heating in NWA 1950. The formation of olivine amorphous lamellae occurs in the shock event with shock pressure of at least over 48.5 GPa and possibly over 56 GPa. The higher shock pressure of NWA 1950 than those of RBT 04261 is consistent with the presence of brown olivine only in NWA 1950 (Takenouchi et al. 2018). The presence of brown olivine throughout the meteorite indicates that the meteorite had experienced high pressure ($\sim 55 \text{ GPa}$) and high postshock temperature ($>900 \text{ }^\circ\text{C}$). Therefore, to summarize the

above discussion, the PDFs of olivine (its width and number density) and its fine-structure (composed of defects or amorphous) are good indicators to estimate the peak shock pressure; defect-rich lamellar PDFs with 0.12–0.14 μm mode width and amorphous lamellar PDFs with >0.2 μm mode width indicate shock pressures higher than 39.5–48.5 GPa and 48.5–56 GPa for RBT 04261 and NWA 1950, respectively.

CONCLUSION

In this study, we performed shock recovery experiments on an olivine-phyric basalt mimicking Martian meteorites to determine shock effects of olivine and also on preheated basalt to investigate the temperature effects on shock features. As a result, we reported following observation results and conclusions:

1. Initial heating before shock recovery experiments promoted lowering of shock pressure for the maskelynitization compared with the experiments at room temperature, which is a consistent result with static experiments (Kubo et al. 2010) and preheated shock recovery experiments using granite and eucrites (Huffman et al. 1993; Yamaguchi et al. 2003).
2. Olivine shocked at 39.5 and 48.5 GPa shows PDFs and similar textures were observed in olivine in RBT 04261 and NWA 1950 while no PDFs formed in olivine shocked ~ 39 GPa at 750 $^{\circ}\text{C}$. Since their mode width and fine-structures (defect-rich or amorphous) were changed as shock pressure increased, they could be good indicators for an estimation of peak shock pressure although we need to consider temperature effects.
3. The estimated minimum peak shock pressures of RBT 04261 and NWA 1950 are 39.5–48.5 GPa and 48.5–56 GPa, respectively, which are consistent with those estimated by postshock temperature expected by the presence of brown olivine (Takenouchi et al. 2018).

Acknowledgment—We thank NIPR (Dr. M. Yasutake and Ms. T. Ojima) for supporting SEM and EBSD works. Dr. T. Sakuyama and Prof. K. Ozawa kindly provided us Kita-Matsuura basalt samples. We also thank the Meteorite Working Group (MWG) for RBT 04261. Mr. H. Yoshida and Mr. K. Ichimura supported electron microprobe works at the Department of Earth and Planetary Science, University of Tokyo. Furthermore, Prof. Kogure and Ms. Fujii kindly helped our FIB-TEM works. T. Shirai helped our shock recovery experiments. Dr. Hu and an anonymous reviewer greatly improve our manuscript by constructive

and helpful comments. We are grateful to associate editor Prof. W. U. Reimold for his handling of the manuscript. This work was supported by JSPS Fellowship to A.T. (15J08812), by NIPR, Research Project Funds KP-307, and by NIPR General Collaboration Project no. 28-30.

Editorial Handling—Dr. W. Uwe Reimold

REFERENCES

- Ashworth J. R. and Barber D. J. 1975. Electron petrography of shock-deformed olivine in stony meteorites. *Earth and Planetary Science Letters* 27:43–50.
- Bauer J. F. 1979. Experimental shock metamorphism of mono- and polycrystalline olivine: A comparative study (abstract). Proceedings of 10th Lunar and Planetary Science Conference. pp. 2573–2596.
- Beck P., Gillet P., El Goresy A., and Mostefaoui S. 2005. Timescales of shock processes in chondritic and Martian meteorites. *Nature* 435:1071–1074.
- Cloos E. 1955. Experimental analysis of fracture patterns. *Bulletin of the Geological Society of America* 66:241–256.
- Duffy T. S. and Ahrens T. J. 1997. Dynamic compression of a Fe-Cr-Ni alloy to 80 GPa. *Journal of Applied Physics* 82:4259–4269.
- Farrell-Turner S., Reimold W. U., Nieuwoudt M., and Erasmus R. M. 2005. Raman spectroscopy of olivine in dunite experimentally shocked to pressures between 5 and 59 GPa. *Meteoritics & Planetary Science* 40:1311–1327.
- Fritz J., Artemieva N., and Greshake A. 2005. Ejection of Martian meteorites. *Meteoritics & Planetary Science* 40:1393–1411.
- Fritz J., Greshake A., and Fernandes V. A. 2017. Revising the shock classification of meteorites. *Meteoritics & Planetary Science* 52:1216–1232. <https://doi.org/10.1111/maps.12845>.
- Goetze C. and Kohlstedt D. L. 1973. Laboratory study of dislocation climb and diffusion in olivine. *Journal of Geophysical Research* 78:5961–5971.
- Goltrant O., Leroux H., Doukhan J.-C., and Cordier P. 1992. Formation mechanism of planar deformation features in naturally shocked quartz. *Physics of the Earth and Planetary Interiors* 74:219–240.
- Greshake A., Fritz J., Böttger U., and Goran D. 2013. Shear-induced ringwoodite formation in the Martian shergottite Dar al Gani 670. *Earth and Planetary Science Letters* 375:383–394.
- Grieve R. A. F., Sharpton V. L., and Stöffler D. 1990. Shocked minerals and the K/T controversy. *Eos, Transactions American Geophysical Union* 71:1792–1793.
- Hu J. and Sharp T. G. 2017. Back-transformation of high-pressure minerals in shocked chondrites: Low-pressure mineral evidence for strong shock. *Geochimica et Cosmochimica Acta* 215:277–294.
- Huffman A. R., Brown J. M., Carter N. L., and Reimold W. U. 1993. The microstructural response of quartz and feldspar under shock loading at variable temperatures. *Journal of Geophysical Research* 98:22,171–22,197.
- Jeanloz R. 1980. Shock effects in olivine and implications for Hugoniot data. *Journal of Geophysical Research* 85:3163–3176.

- Jeanloz R., Ahrens T. J., Lally J. S., Nord G. L. Jr, Christie J. M., and Heuer A. H. 1977. Shock-produced olivine glass: First observation. *Science* 97:457–459.
- Ji C., Levitas V. I., Zhu H., Chaudhuri J., Marathe A., and Ma Y. 2012. Shear-induced phase transition of nanocrystalline hexagonal boron nitride to wurtzitic structure at room temperature and lower pressure. *Proceedings of the National Academy of Sciences* 109:19,108–19,112.
- Kubo T., Kimura M., Kato T., Nishi M., Tominaga A., Kikegawa T., and Funakoshi K. 2010. Plagioclase breakdown as an indicator for shock conditions of meteorites. *Nature Geoscience* 3:41–45. <https://doi.org/10.1038/NCEO704>.
- Ma C. 2018. A closer look at shocked meteorites: Discovery of new high-pressure minerals. *American Mineralogist* 103:1521–1522.
- Mandon M., Guyot F., Peyronneau J., and Poirier J. P. 1989. Electron microscopy of high-pressure phases synthesized from natural olivine in diamond anvil cell. *Physics and Chemistry of Minerals*. 16:320–330.
- Marsh S. P. 1980. *LASL shock Hugoniot data*. Berkeley, California: University of California Press.
- Milton D. J. and DeCarli P. S. 1963. Maskelynite: Formation by explosive shock. *Science* 140:670–671.
- Miyahara M., Ohtani E., Ozawa S., Kimura M., El Goresy A., Sakai T., Nagase T., Hiraga K., Hirao N., and Ohishi Y. 2011. Natural dissociation of olivine to (Mg, Fe)SiO₃ perovskite and magnesiowüstite in a shocked Martian meteorite. *Proceedings of National Academy of Sciences* 108:5999–6003.
- Müller W. F. and Hornemann U. 1969. Shock-induced planar deformation structures in experimentally shock-loaded olivines and in olivines from chondritic meteorites. *Earth and Planetary Science Letters* 7:251–264.
- Ohtani E., Kimura Y., Kimura M., Takata T., Kondo T., and Kubo T. 2004. Formation of high-pressure minerals in shocked L6 chondrite Yamato 791384: Constraints on shock conditions and parent body size. *Earth and Planetary Science Letters* 227:505–515.
- Phakey P., Dollinger G., and Christie J. 1972. Transmission electron microscopy of experimentally deformed olivine crystals. *Flow and Fracture of Rocks, American Geophysical Union, Geophysical Monograph Series* 16:117–138.
- Reimold W. U., and Stöffler D. 1978. Experimental shock metamorphism of dunite. Proceedings, 9th Lunar and Planetary Science Conference. pp. 2805–2824.
- Santamaria-Perez D., Thomson A., Segura A., Pellicer-Torres J., Manjon F. J., Corà F., McColl K., Wilson M., Dobson D., and McMillan P. F. 2016. Metastable structural transformations and pressure-induced amorphization in natural (Mg, Fe)₂SiO₄ olivine under static compression: A Raman spectroscopic study. *American Mineralogist* 101:1642–1650.
- Schmitt R. T. 2000. Shock experiments with the H6 chondrite Kernouvé: Pressure calibration of microscopic shock effects. *Meteoritics & Planetary Science* 35:545–560.
- Sekine T. 1989. Shock-induced phase transformation of graphite-like boron nitride to denser forms. *Journal of Materials Science Letters* 8:872–874.
- Sekine T. 1997. Shock wave chemical synthesis. *European Journal of Solid State Inorganic Chemistry* 34:823–833.
- Sharp T. G. and DeCarli P. S. 2006. Shock effects in meteorites. In *Meteorites and the early solar system II*, edited by Lauretta D. S. and McSween H. Y. Jr. Tucson, Arizona: University of Arizona Press. pp. 653–677.
- Stöffler D., Ostertag R., Jammes C., and Pfannschmidt G. 1986. Shock metamorphism and petrography of the Shergotty achondrite. *Geochimica et Cosmochimica Acta* 50:889–903.
- Stöffler D., Keil K., and Scott E. R. D. 1991. Shock metamorphism of ordinary chondrites. *Geochimica et Cosmochimica Acta* 55:3845–3867.
- Stöffler D., Hamann C., and Metzler K. 2018. Shock metamorphism of planetary silicate rocks and sediments: Proposal for an updated classification system. *Meteoritics & Planetary Science* 53:5–49.
- Syono Y., Goto T., Sato J., and Takei H. 1981. Shock compression measurements of single-crystal forsterite in the pressure range 15–93 GPa. *Journal of Geophysical Research* 86:6181–6186.
- Takenouchi A., Mikouchi T., and Kogure T. 2017. Mineralogical study of brown olivine in Northwest Africa 1950 shergottite and implications for the formation mechanism of iron nanoparticles. *Meteoritics & Planetary Science* 52:2491–2504.
- Takenouchi A., Mikouchi T., and Yamaguchi A. 2018. Shock veins and brown olivine in Martian meteorites: Implications for their shock pressure-temperature histories. *Meteoritics & Planetary Science* 53:2259–2284.
- Tomeoka K., Yamahana Y., and Sekine T. 1999. Experimental shock metamorphism of the Murchison CM carbonaceous chondrite. *Geochimica et Cosmochimica Acta* 63:3683–3703.
- Tomioka N. and Miyahara M. 2017. High-pressure minerals in shocked meteorites. *Meteoritics & Planetary Science* 52:2017–2039. <https://doi.org/10.1111/maps.12902>.
- Treiman A. H., Dyar M. D., McCanta M., Noble S. K., and Pieters C. M. 2007. Martian dunite NWA 2737: Petrographic constraints on geological history, shock events, and olivine color. *Journal of Geophysical Research* 112:E04002. <https://doi.org/10.1029/2006JE002777>
- Usui T., Sanborn M., Wadhwa M., and McSween H. Y. Jr 2010. Petrology and trace element geochemistry of Robert Massif 04261 and 04262 meteorites, the first examples of geochemically enriched lherzolithic shergottites. *Geochimica et Cosmochimica Acta* 74:7283–7306.
- Walton E. L. 2013. Shock metamorphism of Elephant Moraine A79001: Implications for olivine-ringwoodite transformation and the complex thermal history of heavily shocked Martian meteorites. *Geochimica et Cosmochimica Acta* 107:299–315.
- Walton E. L., Sharp T. G., Hu J., and Filiberto J. 2014. Heterogeneous mineral assemblages in Maritan meteorite Tissint as a result of a recent small impact event on Mars. *Geochimica et Cosmochimica Acta* 140:334–348.
- Yamaguchi A., and Sekine T. 2000. Monomineralic mobilization of plagioclase by shock: An experimental study. *Earth and Planetary Science Letters* 175:289–296.
- Yamaguchi A., Sekine T., and Mori H. 2003. Shock experiments on a pre-heated basaltic eucrite. In *High-pressure shock compression of solids V. Shock chemistry with applications to meteorites impacts*, edited by Davison L., Horie Y., and Sekine T. Berlin: Springer Science + Business Media, LLC. pp. 29–45.